Photochemical & Photobiological Sciences

PAPER

CO_2 reduction over $NaNbO_3$ and $NaTaO_3$ perovskite photocatalysts

F. Fresno,*[a] P. Jana,[b] P. Reñones,[a] J. M. Coronado,[b] D. P. Serrano[b,c] and V. A. de la Peña O'Shea*[a]

Received 30th June 2016,
Accepted 19th August 2016

DOI: 10.1039/c6pp00235h

www.rsc.org/pps

The activity of $NaNbO_3$ and $NaTaO_3$ perovskites for the photocatalytic reduction of CO_2 is studied in this work. For this purpose, sodium niobate and tantalate have been prepared using solid-state reactions, extensively characterised by means of powder X-ray diffraction, UV-vis, photoluminescence and Raman spectroscopies and N_2 adsorption isotherms, and tested in the gas-phase reduction of CO_2 under UV light in a continuous flow photoreactor. $NaNbO_3$ is constituted of an orthorhombically distorted perovskite structure, while a *ca.* 4.5 : 1 combination of the orthorhombic and monoclinic modifications is found in the tantalate. Both catalysts exhibit interesting intrinsic activities, with the tantalate material giving rise to a slightly higher performance. This is attributed to a compromise situation between electron–hole recombination and the reducing potential of conduction band electrons. In addition, a decrease in the competition of water protons for photogenerated electrons is observed with both catalysts with respect to TiO_2.

Introduction

A promising strategy for CO_2 utilisation is the production of fuels and chemicals by means of photocatalytic reduction using water as an electron donor. This process, one of those encompassed in artificial photosynthesis (AP), is based on the use of semiconductor catalysts, and is particularly convenient taking into account that reactions are driven under soft conditions (temperature and pressure) and can take advantage of the use of a sustainable energy source.[1] However, although intense effort has been made in the last few years in order to increase the photocatalytic efficiencies of this process, very low quantum yields are still reported in the literature, especially when water is used as the only hole scavenger, without the use of any sacrificial reagent.[2–4] The central role in the overall efficiency of photocatalytic processes is played by the semiconductor photocatalyst, able to generate and manage electron–hole pairs upon irradiation with light of photon energy equal to or greater than its band gap. In order to efficiently promote photocatalytic reactions, semiconductors must have the appropriate thermodynamic (band positions), kinetic (surface chemistry) and stability (lack of deactivation or photocorrosion) characteristics. In this respect, one interesting type of semiconductor photocatalyst for the CO_2 reaction is that formed by ternary oxides with perovskite structure like alkaline niobates and tantalates, which possess a conduction band with sufficiently high energy to transfer electrons to the CO_2 molecule and, at the same time, a valence band with energy low enough to promote water oxidation.[5,6] In addition, these perovskite structures have been revealed in the last few years to be particularly suitable for photocatalytic water splitting and hydrogen production from aqueous solutions of sacrificial reagents.[5–7] In this line, remarkable results have been obtained with $NaNbO_3$, $NaTaO_3$ and modifications of them in H_2 evolution experiments from pure water or with methanol as a hole scavenger.[5–11] Although scarcer, some reports have revealed the potential of these structures for CO_2 photocatalytic reduction.[12–16] In this work, we compare the activities of both types of perovskites obtained under the same synthetic conditions for gas-phase CO_2 reduction under UV light irradiation, with an extensive characterisation of the obtained materials by different physico-chemical techniques.

[a]*Photoactivated Processes Unit, IMDEA Energy Institute, Móstoles Technology Park, Avenida Ramón de la Sagra, 3, 28935 Móstoles, Madrid, Spain. E-mail: fernando.fresno@imdea.org, victor.delapenya@imdea.org*
[b]*Thermochemical Processes Unit, IMDEA Energy Institute, Móstoles Technology Park, Avenida Ramón de la Sagra, 3, 28935 Móstoles, Madrid, Spain*
[c]*Chemical and Environmental Engineering Group, ESCET, Rey Juan Carlos University, c/Tulipán s/n, 28933 Móstoles, Madrid, Spain*

Experimental methods

Synthesis

$NaNbO_3$ and $NaTaO_3$ were synthesised by solid-state reactions. Nb_2O_5 or Ta_2O_5 was carefully ground together with Na_2CO_3; the latter was taken in 5% excess with respect to the

stoichiometric amount to compensate for volatilisation losses. The mixture was then heated in air in a muffle furnace at 900 °C for 12 h, at a heating rate of 10 °C min^{-1}. Commercial anatase-type titanium dioxide (TiO_2, PC500), supplied by CristalACTIV™, was used as an activity reference. Prior to use, TiO_2 was stabilised with a thermal treatment at 400 °C for 4 h.

Characterisation techniques

The chemical composition of the photocatalysts was quantified using an induced coupled plasma atomic emission spectrometer (ICP-AES, Perkin Elmer 2300 DV). Powder X-ray diffraction (XRD) patterns were recorded with a Panalytical EMPYREAN diffractometer using CuK_α radiation (λ = 1.54178 Å) at a scanning rate of 0.01° s^{-1}. N_2 adsorption–desorption isotherms were recorded at −196 °C in a QUADRASORB instrument. A Philips Technai 20 transmission electron microscope, operating with a tungsten filament working at 200 kV, was used to obtain TEM images. Raman spectra were recorded at room temperature using a JASCO NRS-5000/7000 series Raman spectrometer with an excitation wavelength of 532 nm. Diffuse reflectance UV-vis spectra were recorded on a UV/Vis/NIR Perkin Elmer Lambda 1050 spectrometer. Photoluminescence experiments were carried out with a Perkin Elmer LS55 fluorescence spectrometer, using an excitation wavelength of 300 nm and a cut-off filter at 350 nm.

CO_2 reduction experiments

CO_2 photoreduction experiments were conducted in continuous flow mode in a gas-phase stainless steel photoreactor, with an effective volume of 280 mL and provided with a borosilicate window for irradiation. The powdered catalysts (0.1 g) were deposited on glass microfibre filters from aqueous suspensions. Pure carbon dioxide (99.9999%, Praxair) and water (Milli-Q) were fed into the reaction system with a $CO_2 : H_2O$ molar ratio of 7.25 by means of a Controlled Evaporator Mixer (CEM). The reaction conditions were set at 2 bar and 50 °C. Irradiation was provided by four UV fluorescent lamps of 6 W each (λ_{max} = 365 nm). In-line analyses of the reactor outlet gas were performed every 22 minutes using an Agilent 7890A gas chromatograph equipped with three columns (BR-Q Plot, BR-Molsieve 5A and CP-Sil 5B), three detectors (2 FID and 1 TCD) and a methaniser.

The reactor was firstly degassed at 50 °C under vacuum and then purged with Ar (100 mL min^{-1}) for 1 h in order to remove any residual compounds weakly adsorbed on the surface of the catalyst. Then a CO_2 and H_2O mixture was fed in the dark for 1 h in order to establish an adsorption–desorption balance at the reaction temperature. Prior to illumination, the reactor was pressurised and kept at the reaction flow rate for another 1 h. All photocatalytic tests were carried out for a period of 15 h of irradiation.

Results and discussion

Characterisation of the photocatalysts

Table 1 summarises the main physicochemical characteristics of $NaNbO_3$ and $NaTaO_3$ photocatalysts. Chemical analyses indicate a good agreement of the obtained compositions with those pursued in the synthetic method (stoichiometric wt% given in brackets in Table 1), with a small defect of sodium that reveals that there still exists an effect of Na volatilisation in spite of the excess of Na_2CO_3 used in the synthesis.

X-ray diffraction patterns of the obtained materials (Fig. 1) show their characteristic crystalline structure.[17] Thus, the $NaNbO_3$ sample is composed of a single phase with an orthorhombically distorted perovskite structure ($NaNbO_3$, ICDD PDF # 01-073-0803). This orthorhombic structure (ICDD PDF # 01-073-0878) is also mainly present in $NaTaO_3$ together with a monoclinically distorted perovskite structure ($NaTaO_3$, ICDD PDF # 01-074-2478), with a minor contribution of an additional hexagonal phase (natrotantite $Na_2Ta_4O_{11}$, ICDD PDF # 01-084-0810). The results of Rietveld refinement of the powder diffractograms of the above mentioned structures are included in Table 1. The natrotantite phase is present in a *ca.* 2.5% amount in the $NaTaO_3$ sample, which contains a *ca.* 4.5 : 1 orthorhombic/monoclinic $NaTaO_3$ proportion. Only slight deviations (maximum 0.15%) exist in cell parameters with respect to the reference structures. Large crystal sizes are found in both metallates, as could be expected considering that they were obtained by solid-state synthesis at high temperature. These large sizes are confirmed by TEM images, an example of which is shown in Fig. 2. In agreement with this, both catalysts present low surface areas, with values around

Table 1 Physicochemical properties of the obtained photocatalysts

	$NaNbO_3$	$NaTaO_3$		
Na (wt%)	13.2 ± 0.4 [14.0]	8.2 ± 0.3 [9.1]		
Nb or Ta (wt%)	59.0 ± 1.2 [56.7]	75.5 ± 1.5 [71.8]		
BET surface area (m^2 g^{-1})	1.0	1.1		
E_g (eV)	3.30	4.05		
Crystalline phase	Orthorhombic $NaNbO_3$	Orthorhombic $NaTaO_3$	Monoclinic $NaTaO_3$	Hexagonal $Na_2Ta_4O_{11}$
Phase mass %	100	80.3	17.3	2.4
Lattice parameters (Å, °)	a = 5.504	a = 5.480	a = 3.889	$a = b$ = 6.208
	b = 5.568	b = 7.791	b = 3.895	
	c = 15.51	c = 5.522	c = 3.891	c = 36.609
			β = 90.398	
Crystal size (nm)	178	160	165	200

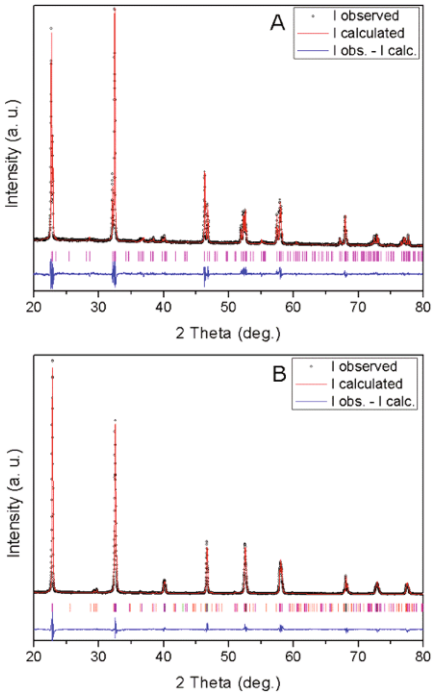

Fig. 1 XRD patterns and profile fits of (A) $NaNbO_3$ and (B) $NaTaO_3$. Vertical lines show the Bragg reflections corresponding to the refined phases (see text and Table 1).

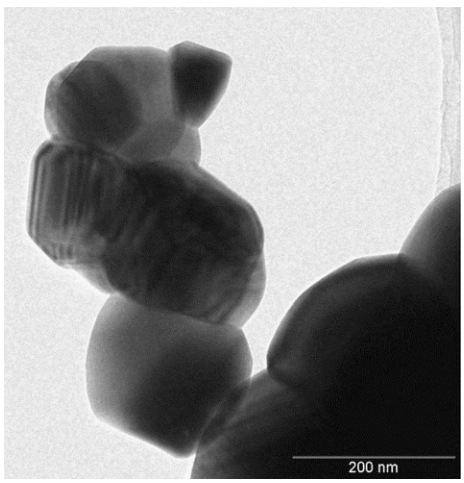

Fig. 2 TEM image of $NaTaO_3$.

1 m^2 g^{-1}. In accordance with the synthesis temperature, the nitrogen adsorption isotherms (not shown) are of type-II in both cases, indicating that the solids are not porous and that the specific surface area is due to the external surface of the particles.

The structural characterisation was complemented by Raman spectroscopy (Fig. 3). The bands in the Raman spectra are well matched with those described in the literature for $NaNbO_3$ [18,19] and $NaTaO_3$.[20] Typical spectral profiles of perovskite structures, with intense bands in the 100–300 and

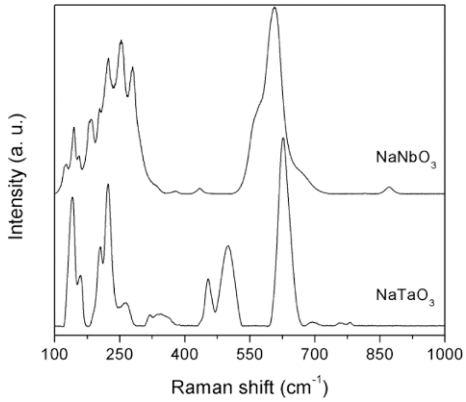

Fig. 3 Raman spectra of the synthesized photocatalysts.

400–700 cm^{-1} regions, are observed. Thus, the $NaNbO_3$ spectrum shows bands at 125, 144 and 155 cm^{-1} corresponding to the librational modes of the NbO_6 octahedra. The rest of the observed bands are generated by the internal vibrations of the NbO_6 octahedra, with the triply degenerate F_{2u} and F_{2g} modes giving rise to the profile observed in the 170–300 cm^{-1} region, and the intense shouldered band centered at 605 cm^{-1}, which is assignable to symmetric stretching modes. The low intensity bands observed at *ca.* 380 and 435 cm^{-1} are indicative of a tilting angle between adjacent octahedra that deviates the $NaNbO_3$ crystalline phase from the ideal perovskite structure, as observed in the X-ray diffractograms discussed above.[21] Also in line with the XRD data for $NaNbO_3$, the weak band at 870 cm^{-1} corresponds to a combination mode in centrosymmetric space goups.[22] Similar assignments can be made for $NaTaO_3$. The spectrum presents bands at 140, 160, 204, and 222 cm^{-1} that are characteristic of Na translational vibration modes, which in the case of $NaNbO_3$ appear at Raman shifts below 100 cm^{-1} and are not observed due to the used Rayleigh filter.[18] The bands at 263, 318 and 345 cm^{-1} can be assigned to the bending modes of TaO_6 octahedra, and those at 453, 499, and 626 cm^{-1} correspond to Ta–O stretching modes, with possible combination bands appearing at 693 and above 750 cm^{-1}. This band distribution is in good agreement with the main presence of an orthorhombic $NaTaO_3$ phase in this catalyst.[23]

Fig. 4 shows the diffuse reflectance UV-vis spectra of $NaNbO_3$ and $NaTaO_3$. As expected, the sharp absorption edge for $NaTaO_3$ appears at a higher energy than in the case of $NaNbO_3$.[5,7,12–16] Their corresponding band gap (E_g) values, included in Table 1, were calculated from Tauc plots considering a direct transition in $NaTaO_3$, in accordance with the main contribution of the orthorhombic phase,[24] and an indirect transition in the case of $NaNbO_3$.[25] The obtained values are in good accordance with those described in the literature for these phases.[12–16,24,25] The valence band potentials of $NaTaO_3$ and $NaNbO_3$ are similar because both consist of O_{2p} orbitals and the oxygen anions coordinate to Ta^{5+} or Nb^{5+} ions, which have the same ionic radius.[8] Hence the difference in the band gaps arises from the higher energy (more negative reduction

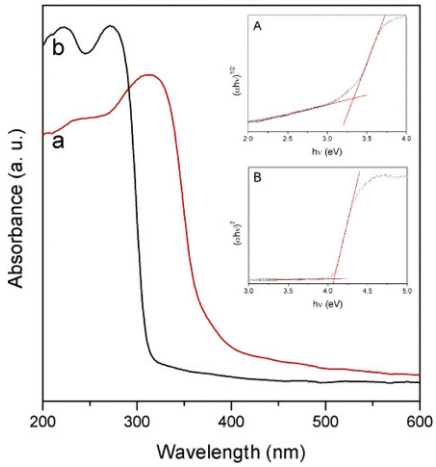

Fig. 4 UV-vis diffuse reflectance spectra of $NaNbO_3$ (a) and $NaTaO_3$ (b). Insets: Tauc plots for $NaNbO_3$ (A) and $NaTaO_3$ (B).

potential) of Ta 5d orbitals, forming the conduction band of $NaTaO_3$, with respect to Nb 4d orbitals forming the conduction band of $NaNbO_3$. Assuming that the valence band potentials in oxides with metal ions without partially filled d levels lie at 2.94 V *vs.* SHE within 2% deviation,[8,26] a band potential diagram like that shown in Fig. 5 can be deduced from the E_g values obtained from UV-vis spectra.

In agreement with the absorption spectra, photoluminescence (PL) measurements (Fig. 6) show a slight displacement of the band-to-band recombination emission (only the tail of which is observed due to the used cut-off filter) to lower wavelength when moving from $NaNbO_3$ to $NaTaO_3$. The low-energy part of the spectra is composed of a broad emission band in the 400–600 cm^{-1} region, as is generally observed in ABO_3 perovskites,[27,28] and is formed by several contributions related to excitons and oxygen vacancies. In this region, it is observed that the PL intensity is lower in $NaNbO_3$, which in general terms can be related to slower electron–hole recombination.[29]

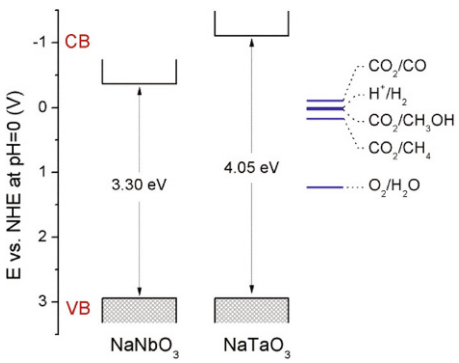

Fig. 5 Schematic representation of the band potentials of $NaNbO_3$ and $NaTaO_3$. Relevant CO_2 reduction potentials have been taken from ref. 33.

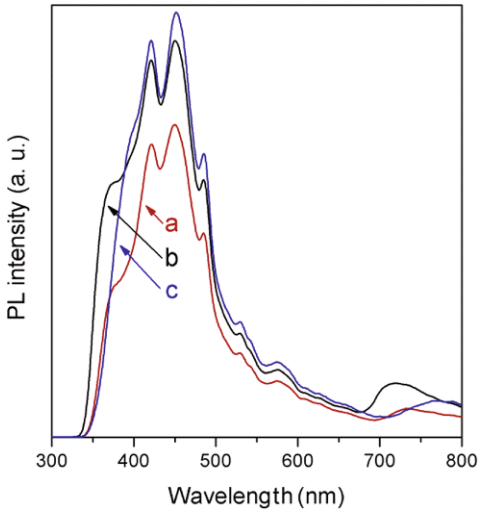

Fig. 6 Photoluminescence spectra of $NaNbO_3$ (a), $NaTaO_3$ (b) and TiO_2 (c).

Photocatalytic activity for CO_2 reduction

Fig. 7 shows the accumulated amounts of the main reaction products over 15 h of irradiation, compared to those obtained with TiO_2 PC500 (S_{BET} = 165.8 m^2 g^{-1}). In all cases, the main CO_2 reduction products are CO, CH_4 and CH_3OH, together with H_2 coming from the concomitant reduction of water competing with that of CO_2. Trace amounts of other products like C_{2+} hydrocarbons and ethanol are obtained, with similar amounts for different catalysts. Reactions carried out in an argon atmosphere under irradiation gave rise to product evolution of less than 2% with respect to the tests performed feeding CO_2 + H_2O, indicating that the evolved gases in the presence of CO_2 and H_2O do not arise from adventitious carbon contamination on the surface of the photocatalysts.

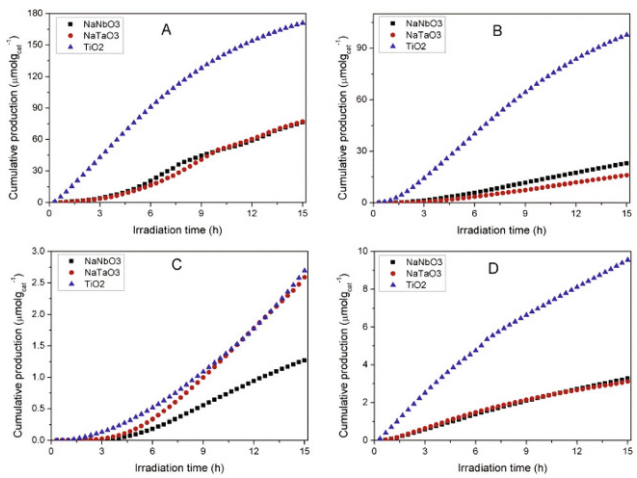

Fig. 7 Evolution of the main products obtained in the photocatalytic reduction of CO_2 over $NaNbO_3$, $NaTaO_3$ and TiO_2: (A) CO, (B) H_2 (C) CH_4, (D) CH_3OH.

In spite of their low surface areas (see Table 1), both $NaNbO_3$ and $NaTaO_3$ give rise to product amounts comparable to those with titania, although the production attained with the latter is considerably larger in all cases except for CH_4. However, if the results are referred to the surface area unit, which would reflect the intrinsic photoactivity of the materials, the production with the synthesised metallates reveals considerable interest. In line with this, the measured PL spectrum of TiO_2 (Fig. 6), with slightly higher intensity than those of both perovskite materials, reveals that the larger net production with titania cannot be explained only in terms of photogenerated charge carrier utilisation.

The comparison of $NaNbO_3$ and $NaTaO_3$ shows very similar production of CO and CH_3OH, with the latter giving rise to a larger amount of CH_4 and a lower amount of H_2. Overall, the total amount of carbon products is slightly larger (*ca.* 2%) for sodium tantalate. In comparative terms, the production results reported here for $NaNbO_3$ and $NaTaO_3$ are competitive with those previously reported for this kind of structure, especially if production normalised to a specific surface area is considered.[12–16]

Fig. 8 depicts the selectivities towards the main reaction products obtained with the different catalysts, calculated on the basis of these products only. The high selectivity to CO rather than to highly reduced carbon products (*e.g.* CH_4) is a common characteristic of oxide photocatalysts without the presence of a metal co-catalyst.[30] In the case of TiO_2 this CO selectivity comes together with a considerable production of H_2 due to a hardly avoidable competition for conduction band electrons by CO_2 and H_2O molecules.[31,32] In the case of the metallates reported here, the selectivity towards carbon monoxide is even increased with respect to titania, and this comes mainly at the expense of hydrogen production as observed in Fig. 8. Therefore, the mentioned electron competition is interestingly shifted towards the reduction of CO_2 with the present catalysts, and is especially remarkable in the case of $NaTaO_3$. A similar observation can be made regarding the selectivity of this catalyst towards methane, which is twice that obtained with both $NaNbO_3$ and TiO_2.

Therefore, it is demonstrated here that, in spite of the low surface area obtained by means of the solid-state synthetic method, both $NaNbO_3$ and $NaTaO_3$ perovskites exhibit interesting intrinsic activities for the photocatalytic reduction of CO_2 under UV irradiation. The comparison of the photoactivity of these metallates and their opto-electronic properties reveals the effect of opposed factors: on the one hand, $NaNbO_3$ presents a lower electron–hole recombination as revealed by its PL spectrum (Fig. 5); on the other hand, as explained in the discussion of UV-vis spectra and displayed in Fig. 5, the electrons in the conduction band of $NaTaO_3$ have a higher energy (more negative reduction potential) than those in $NaNbO_3$, which implies a larger driving force for reduction reactions.[33] Similar observations in this last respect have been made in photocatalytic hydrogen production reactions.[8,9,11] As a result of these two factors, both perovskites give rise to similar conversions in the CO_2 reduction reaction, with slightly higher carbon product evolution over $NaTaO_3$.

Regarding structural aspects, the presence of a monoclinic phase in the $NaTaO_3$ sample may also play a role in its photocatalytic performance. According to the literature,[34] the monoclinic phase of $NaTaO_3$ leads to a Ta–O–Ta angle closer to 180°, more favourable for charge delocalisation. In addition, some authors have proposed a positive effect of multi-phase $NaTaO_3$ samples for CH_4 evolution in the photocatalytic reduction of CO_2.[15]

An additional interesting feature of these photocatalysts is their lower selectivity towards hydrogen with respect to TiO_2, which suggests that these structures drive the competition between CO_2 and H_2O for conduction band electrons towards the reduction of carbon dioxide. This result is especially remarkable in the case of $NaTaO_3$, which also shows higher methane selectivity.

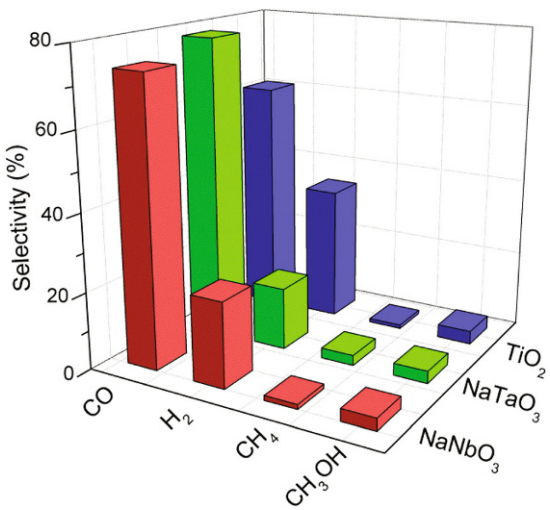

Fig. 8 Selectivities towards the main products obtained in the photocatalytic reduction of CO_2 over $NaNbO_3$, $NaTaO_3$ and TiO_2.

Conclusions

$NaNbO_3$ and $NaTaO_3$ perovskite photocatalysts have been prepared by solid-state reactions, extensively characterised and tested for the reduction of CO_2. X-ray diffraction studies reveal the niobate material to be composed of an orthorhombically distorted perovskite structure, while the tantalate is mainly formed by a *ca.* 4.5 : 1 combination of the orthorhombic and monoclinic modifications. In spite of their low surface area, both catalysts exhibit interesting intrinsic activities for the photocatalytic reduction of CO_2 under UV irradiation, with the tantalate material giving rise to a slightly higher performance attributed to a compromise situation between photogenerated electron–hole utilisation and the reducing potential of conduction band electrons. Interestingly, both $NaNbO_3$ and $NaTaO_3$ seem to drive the competition between CO_2 and H_2O for conduction band electrons towards the reduction of carbon

dioxide, as reflected by a lower selectivity to H_2 in the photocatalytic process. This result is especially remarkable in the case of sodium tantalate.

Acknowledgements

This work has received financial support from the Spanish Ministry of Economy and Competitiveness through the projects *Hybrid-Leaf* (CTQ2014-51487-ERC) and *SolarFuel* (ENE2014-55071-JIN) and from the Region of Madrid (program *MAD2D*, S2013/MIT-3007). F. F. acknowledges financial support from the *Amarout-II* PEOPLE-COFUND Marie Skłodowska-Curie Action (REA grant agreement no. 291803). Support from the Repsol Technology Centre is gratefully acknowledged.

Notes and references

1 V. A. de la Peña O'Shea, D. P. Serrano and J. M. Coronado, in *Molecules to Materials. Pathways to Artificial Photosynthesis*, ed. E. Rozhkova and K. Ariga, Springer, London, 2015, pp. 171–191.

2 S. Protti, A. Albini and N. Serpone, Photocatalytic generation of solar fuels from the reduction of H_2O and CO_2: a look at the patent literature, *Phys. Chem. Chem. Phys.*, 2014, **16**, 19790–19827.

3 F. Fresno, R. Portela, S. Suárez and J. M. Coronado, Photocatalytic materials: recent achievements and near future trends, *J. Mater. Chem. A*, 2014, **2**, 2863.

4 L. Yuan and Y.-J. Xu, Photocatalytic conversion of CO_2 into value-added and renewable fuels, *Appl. Surf. Sci.*, 2015, **342**, 154–167.

5 F. E. Osterloh, Inorganic materials as catalysts for photochemical splitting of water, *Chem. Mater.*, 2008, **20**, 35–54.

6 P. Kanhere and Z. Chen, A review on visible light active perovskite-based photocatalysts, *Molecules*, 2014, **19**, 19995–20022.

7 M. D. Hernández-Alonso, F. Fresno, S. Suárez and J. M. Coronado, Development of alternative photocatalysts to TiO_2: challenges and opportunities, *Energy Environ. Sci.*, 2009, **2**, 1231–1257.

8 H. Kato and A. Kudo, Water splitting into H_2 and O_2 on alkali tantalate photocatalysts $ATaO_3$ (A=Li, Na, and K), *J. Phys. Chem. B*, 2001, **105**, 4285–4292.

9 J. W. Liu, G. Chen, Z. H. Li and Z. G. Zhang, Hydrothermal synthesis and photocatalytic properties of $ATaO_3$ and $ANbO_3$ (A=Na and K), *Int. J. Hydrogen Energy*, 2007, **32**, 2269–2272.

10 P. Jana, C. Mata Montero, P. Pizarro, J. M. Coronado, D. P. Serrano and V. A. de la Peña O'Shea, Photocatalytic hydrogen production in the water/methanol system using Pt/RE:$NaTaO_3$ (RE=Y, La, Ce, Yb) catalysts, *Int. J. Hydrogen Energy*, 2014, **39**, 5283–5290.

11 P. Jana, V. A. de la Peña O'Shea, C. Mata Montero, P. Gálvez, P. Pizarro, J. M. Coronado and D. P. Serrano, Mixed $NaNb_xTa_{1-x}O_3$ perovskites as photocatalysts for H_2 production, *Green Chem.*, 2015, **17**, 1735–1743.

12 H. Shi, G. Chen, C. Zhang and Z. Zou, Polymeric g-C3N4 coupled with $NaNbO_3$ nanowires toward enhanced photocatalytic reduction of CO_2 into renewable fuel, *ACS Catal.*, 2014, **4**, 3637–3643.

13 H. Shi, T. Wang, J. Chen, C. Zhu, J. Ye and Z. Zou, Photoreduction of carbon dioxide over $NaNbO_3$ nanostructured photocatalysts, *Catal. Lett.*, 2011, **141**, 525–530.

14 H. Zhou, P. Li, J. Guo, R. Yan, T. Fan, D. Zhang and J. Ye, Artificial photosynthesis on tree trunk derived alkaline tantalates with hierarchical anatomy: towards CO_2 photofixation into CO and CH_4, *Nanoscale*, 2015, **7**, 113–120.

15 P. Li, H. Xu, L. Liu, T. Kako, N. Umezawa, H. Abe and J. Ye, Constructing cubic-orthorhombic surface-phase junctions of $NaNbO_3$ towards significant enhancement of CO_2 photoreduction, *J. Mater. Chem. A*, 2014, **2**, 5606–5609.

16 M. Li, P. Li, K. Chang, T. Wang, L. Liu, Q. Kang, S. Ouyang and J. Ye, Highly efficient and stable photocatalytic reduction of CO_2 to CH_4 over Ru loaded $NaTaO_3$, *Chem. Commun.*, 2015, **51**, 7645–7648.

17 A. Torres-Pardo, R. Jiménez, E. García-González and J. M. González-Calbet, Phase coexistence in $NaNb_{(1-x)}Ta_xO_3$ materials with enhanced dielectric properties, *J. Mater. Chem.*, 2012, **22**, 14938–14943.

18 Y. Shiratori, A. Magrez, J. Dornseiffer, F.-H. Haegel, C. Pithan and R. Waser, Polymorphism in micro-, submicro-, and nanocrystalline $NaNbO_3$, *J. Phys. Chem. B*, 2005, **109**, 20122–20130.

19 G. Li, T. Kakoa, D. Wanga, Z. Zoub and J. Ye, Composition dependence of the photophysical and photocatalytic properties of $(AgNbO_3)_{1-x}(NaNbO_3)_x$ solid solutions, *J. Solid State Chem.*, 2007, **180**, 2845–2850.

20 S. P. Phivilay, A. A. Puretzky, K. Domen and I. E. Wachs, Nature of catalytic active sites present on the surface of advanced bulk tantalum mixed oxide photocatalysts, *ACS Catal.*, 2013, **3**, 2920–2929.

21 J.-M. Jehng and I. E. Wachs, Structural chemistry and Raman spectra of niobium oxides, *Chem. Mater.*, 1991, **3**, 100–107.

22 V. Shanker, S. L. Samal, G. K. Pradhan, C. Narayana and A. K. Ganguli, Nanocrystalline $NaNbO_3$ and $NaTaO_3$: Rietveld studies, Raman spectroscopy and dielectric properties, *Solid State Sci.*, 2009, **11**, 562–569.

23 N. G. Teixeira, A. Dias and R. L. Moreira, Raman scattering study of the high temperature phase transitions of $NaTaO_3$, *J. Eur. Ceram. Soc.*, 2007, **27**, 3683–3686.

24 W.-H. Lin, C. Cheng, C.-C. Hu and H. Teng, $NaTaO_3$ photocatalysts of different crystalline structures for water splitting into H_2 and O_2, *Appl. Phys. Lett.*, 2006, **89**, 211904.

25 P. Li, S. Ouyang, Y. Zhang, T. Kako and J. Ye, Surface-coordination-induced selective synthesis of cubic and orthorhombic $NaNbO_3$ and their photocatalytic properties, *J. Mater. Chem. A*, 2013, **1**, 1185–1191.

26 D. E. Scaife, Oxide semiconductors in photoelectrochemical conversion of solar energy, *Sol. Energy*, 1980, **25**, 41–54.
27 G. F. Teixeira, T. R. Wright, D. C. Manfroi, E. Longo, J. A. Varela and M. A. Zaghete, Photoluminescence in $NaNbO_3$ particles and films, *Mater. Lett.*, 2015, **139**, 443–446.
28 Y.-C. Lee, H. Teng, C.-C. Hu and S.-Y. Hu, Temperature-dependent photoluminescence in $NaTaO_3$ with different crystalline structures, *Electrochem. Solid-State Lett.*, 2008, **11**, P1–P4.
29 J. Liqiang, Q. Yichun, W. Baiqi, L. Shudan, J. Baojiang, Y. Libin, F. Wei, F. Honggang and S. Jiazhong, Review of photoluminescence performance of nano-sized semiconductor materials and its relationships with photocatalytic activity, *Sol. Energy Mater. Sol. Cells*, 2006, **90**, 1773–1787.
30 S. Xie, Q. Zhang, G. Liu and Y. Wang, Photocatalytic and photoelectrocatalytic reduction of CO_2 using heterogeneous catalysts with controlled nanostructures, *Chem. Commun.*, 2016, **52**, 35–59.
31 L. Collado, P. Jana, B. Sierra, J. M. Coronado, P. Pizarro, D. P. Serrano and V. A. de la Peña O'Shea, Enhancement of hydrocarbon production via artificial photosynthesis due to synergetic effect of Ag supported on TiO_2 and ZnO semiconductors, *Chem. Eng. J.*, 2013, **224**, 128–135.
32 L. Collado, A. Reynal, J. M. Coronado, D. P. Serrano, J. R. Durrant and V. A. de la Peña O'Shea, Effect of Au surface plasmon nanoparticles on the selective CO_2 photoreduction to CH_4, *Appl. Catal., B*, 2015, **178**, 177–185.
33 X. Li, J. Yu and M. Jaroniec, Hierarchical photocatalysts, *Chem. Soc. Rev.*, 2016, **45**, 2603–2636.
34 C. C. Hu, C. C. Tsai and H. Teng, structure characterization and tuning of perovskite-like $NaTaO_3$ for applications in photoluminescence and photocatalysis, *J. Am. Ceram. Soc.*, 2009, **92**, 460–466.